

Revisiting the Statistics of X-ray Flares in Gamma-ray Bursts

Y. Wang^{1,2}, Y. Aimuratov^{1,2,4}, R. Moradi^{1,2}, M. Peresano³, R. Ruffini^{1,2,4,5}, and S. Shakeri^{2,6}

- ¹ ICRA and Dipartimento di Fisica, Sapienza Università di Roma, P.le Aldo Moro 5, 00185 Rome, Italy
- ² ICRANet, P.zza della Repubblica 10, 65122 Pescara, Italy
- ³ Università degli Studi di Udine, via delle Scienze 206, 33100 Udine, Italy
- ⁴ Université de Nice Sophia Antipolis, CEDEX 2, Grand Château Parc Valrose, Nice, France
- ⁵ ICRANet-Rio, Centro Brasileiro de Pesquisas Físicas, Rua Dr. Xavier Sigaud 150, 22290–180 Rio de Janeiro, Brazil
- ⁶ School of Astronomy, Institute for Research in Fundamental Sciences (IPM), P.O. Box 19395-5531, Tehran, Iran e-mail: yu.wang@icranet.org

Abstract. The statistics of X-ray flares in the afterglow of gamma-ray bursts (GRBs) have been studied extensively without considering the possible different origins of each flare. By satisfying six observational criteria, we find a sample composed of 16 long GRBs observed by *Swift* satellite may share a same origin. By applying the Markov chain Monte Carlo iteration and the machine learning algorithms (locally weighted regression and Gaussian process regression), impressively, the flares in these GRBs show strong correlations with the energy released in the prompt emission. These correlations were never discovered in previous papers, and they could not be well explained by previous models. These correlations imply that the prompt emission and the X-ray flare are not independent, they may be originated following a same sequence. The new THESUS satellite will provide us a larger sample and more detailed spectra to refine the results we obtained in this article.

Key words. gamma-ray burst: general — methods: statistical — machine learning

1. Introduction

GRBs are complex authentic astrophysical laboratories encompassing different families, originating in different progenitors, and each characterized by different physical and astrophysical regimes. Dezalay et al. (1992); Kouveliotou et al. (1993) classified GRBs into short or long classes due to the duration of the

prompt emission, Ruffini et al. (2015, 2016) proposed several families of GRBs based on their different configurations of binary systems.

The observed time sequence of a typical long GRB starts from the trigger time given by an instrument on-board of a satellite, often *Swift*-BAT or *Fermi*-GBM. Later the instrument registers a very intense emission, prompt

emission, lasting tens of seconds, and constituted by one or more pulses. This emission contains the majority of the GRB energy in hard X-ray and gamma-ray. Then comes the afterglow, observed by Swift-XRT in the soft X-ray band, and several telescopes in the optical and radio bands. Afterglow starts, following the tail of prompt emission, with one or more flares superposing, these flares last some hundred of seconds. Then a shallow decay or a plateau during the time range 10^2 - 10^6 s. Later the light curve decays again with a powerlaw index ~ -1.2 (Zhang et al. 2006). During the prompt emission and the afterglow, a few GRBs observed high energy GeV photons by Fermi-LAT (Ackermann et al. 2013). The observation ceases commonly in a few days or months. In this paper, we concentrate on the X-ray flares in the early afterglow and their relations with the aforementioned processes.

Flares in the afterglow appear approximately in half of the observed GRBs (Wang & Dai 2013), some of which have more than one flare. Flares mostly arise in the early afterglow (< 1000s), while only a few are observed in the very late time ($> 10^4s$). Chincarini et al. (2007) fitted more than 60 X-ray flares of short and long GRBs together, most of them have no detection of redshift, they found the duration of flares and their peak time are faintly correlated, and that the subgroup of them occurring earlier than 1000 s can hardly form a correlation. Curran et al. (2008) classified flares into early and late groups, and their result confirms Chincarini et al. (2007).

In this paper¹, our approach is not to improve on the existing statistical analysis containing as more flares as possible. Instead we are open to a more selective vision that very distinct patterns of flares can be observed, and consequently the underlying mechanisms causing similar morphologies can be identi-

fied. We consequently select a group of flares sharing some similarities, and fulfilling our criteria (Section 2). We analyze the flares and general features of these GRBs. Our sample shows clear new correlations, some of which are not prominent if adopting all the flares (Section 3). We discuss that the previous models lacks the capacity of interpreting our findings (Section 4).

2. Sample Preparation

We adopt a machine learning algorithm named locally weighted regression ², similar sample is obtained from Swenson et al. (2013) which applied the Bayesian Information method. Additionally, we filter the GRBs again by applying 6 model independent criteria. Our purpose of these criteria follows:

Most previous papers adopt all the GRBs, even without known redshift, this is inappropriate to analyze the physical origins, especially for high redshift GRBs.

Most previous papers analyze all the x-ray flares together, which ignores possible findings and correlations existing in specific subclasses of GRBs.

We intend to collect a sample of flares possibly from a same mechanism. We start from the GRBs with known redshift, since we care most the intrinsic mechanism. Then we make two hypotheses to be justified, and our criteria are based on the hypotheses.

Hypothesis 1: Flares with distinct observed patterns could be produced by various mechanisms. So we select select flares sharing similar morphologies, which brings two criteria:

Criterion 1: Flares in the long GRBs. Criterion 2: Flares occurring before the plateau phase: early time flare.

Hypothesis 2: X-ray flares could be generated differently from the prompt spikes, which also brings two criteria:

¹ The data analysis of this work was performed during the Swift data reduction seminar given by Y. Wang in ICRANet under the supervision of R. Ruffini. Y. Aimuratov, R. Moradi, M. Peresano and S. Shakeri attended the seminar and all contributed to this work. Related material has been published on http://grb.physical.reviews/en/latest/XRT.html

https://github.com/YWangScience/ AstroNeuron

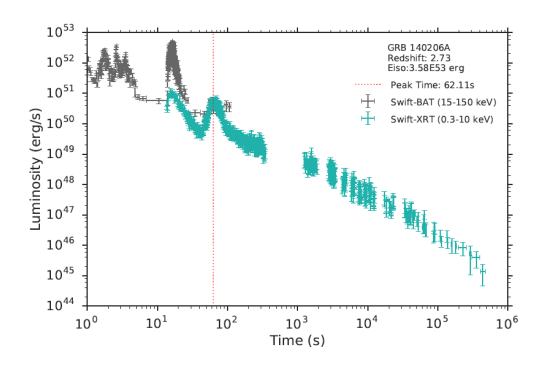


Fig. 1. Light-curve of GRB 140206A: This GRB was detected by Swift (Lien et al. 2014). The Swift-BAT light curve shows a multi-peaked structure with roughly three main pulses (Sakamoto et al. 2014). The redshift, as observed by NOT (Malesani et al. 2014) is z = 2.73, and the isotropic energy is $E_{iso} =$ 3.58×10^{53} erg. GRB 140206A has two flares in Swift-XRT. A gamma-ray flare coincides with the last Swift-BAT spike at ~ 18 s having a spectral of power-law index -0.88 ± 0.03 , most of the energy is contributed by the hard X-ray and the gamma-ray photons. The second flare at 62.11 s with a power-law index -1.73 ± 0.06 is the flare that we are interested in this paper, most of its energy is in the soft X-ray band. The light-curve is plotted in the cosmological rest-frame, k-correction is dually applied.

Criterion 3: Exclude flares that other bands dominate the soft X-ray band.

Criterion 4: Exclude flares contaminated by the prompt emission.

Also in order to do reliable data analysis, we consider

Criterion 5: Obvious flare: luminosity at the peak of the flare must be more than double of the underlying light curve, and the signal to noise ratio (SNR) in the flare >10.

Criterion 6: Swift X-ray light-curve is complete till 10⁴ s in the cosmological rest-frame.

Surveying 421 Swift GRBs with redshift till the end of 2016 year, we find 16 GRBs sat-

isfying all the criteria. Among them, 7 GRBs show a single X-ray flare. The other 9 GRBs contain two flares, generally we exclude the first one by Criterion 3. This sample covers a wide range of redshift. GRB 070318 is the closest one with redshift z=0.84, GRB 090516A with redshift z=4.11 is the farthest one. The isotropic energy E_{iso} also spreads a wide range: 5 GRBs have E_{iso} of the order of 10^{52} erg, 9 GRBs have E_{iso} the order of 10^{53} erg, and 2 GRBs have extremely high $E_{iso} > 10^{54}$ erg. Therefore, we consider this sample is well-constructed. We give an example of the a selected GRB 140206A in figure 1

3. Statistical Correlation

Physical mechanisms are reflected by observations, from which the most direct and obvious observables are energy and time. If our sample really reflects some physical processes, there shall exist some correlations between energy and time, or between themselves.

A GRB's energy is usually measured by the isotropic energy E_{iso} , which assumes that the prompt emission to be isotropic and is computed by integrating the prompt photons in the energy range from 1 KeV to 10 MeV Bloom et al. (2001). In our sample, *Swift* has data for all the GRBs, *Konus-Wind* observed GRB 080607, 080810, 090516A, 131030A, 140419A, 141221A and 151027A, while *Fermi* detected GRB 090516A, 140206, 141221A, 151027A (these 4 *Fermi* GRBs have no prominent GeV emission with likelihood test statistic TS < 20).

None of the satellite is able to cover the entire 1 KeV to 10 MeV energy band of E_{iso} , we need to fit the spectrum and find the best model, then extrapolate the integration of energy by the model. This method is relatively safe for GRBs observed by *Fermi* and *Konus-Wind*, but 8 GRBs in our sample have been observed only by *Swift*, so we uniformly fit and extrapolate these 8 GRBs by power-law and cutoff power-law, then we take the average

³ The entire luminosity light-curves of the 16 GRBs are shown in Ruffini et al. (2018)

| CDD | | - | | * / / | | |
|---------|--------|---------------------------------|--------------------|---------------------------------|-------------------|---------------------------------|
| GRB | Z | E_{iso} (erg) | t_p (s) | L_p (erg/s) | Δt (s) | E_f (erg) |
| 060204B | 2.3393 | $2.93(\pm0.60) \times 10^{53}$ | 100.72 ± 6.31 | $7.35(\pm 2.05) \times 10^{49}$ | 17.34 ± 6.83 | $8.56(\pm 0.82) \times 10^{50}$ |
| 060607A | 3.082 | $2.14(\pm 1.19) \times 10^{53}$ | 66.04 ± 4.98 | $2.28(\pm0.48) \times 10^{50}$ | 18.91 ± 3.84 | $3.33(\pm0.32) \times 10^{51}$ |
| 070318 | 0.84 | $3.41(\pm 2.14) \times 10^{52}$ | 154.7 ± 12.80 | $6.28(\pm 1.30) \times 10^{48}$ | 63.80 ± 19.82 | $3.17(\pm 0.37) \times 10^{50}$ |
| 080607 | 3.04 | $1.87(\pm 0.11) \times 10^{54}$ | 37.48 ± 3.60 | $1.14(\pm 0.27) \times 10^{51}$ | 15.63 ± 4.32 | $1.54(\pm 0.24) \times 10^{52}$ |
| 080805 | 1.51 | $7.16(\pm 1.90) \times 10^{52}$ | 48.41 ± 5.46 | $4.66(\pm 0.59) \times 10^{49}$ | 27.56 ± 9.33 | $9.68(\pm 1.24) \times 10^{50}$ |
| 080810 | 3.35 | $5.00(\pm0.44) \times 10^{53}$ | 51.03 ± 6.49 | $1.85(\pm 0.53) \times 10^{50}$ | 12.38 ± 4.00 | $1.80(\pm 0.17) \times 10^{51}$ |
| 081008 | 1.967 | $1.35(\pm0.66) \times 10^{53}$ | 102.24 ± 5.66 | $1.36(\pm 0.33) \times 10^{50}$ | 18.24 ± 3.63 | $1.93(\pm 0.16) \times 10^{51}$ |
| 081210 | 2.0631 | $1.56(\pm0.54) \times 10^{53}$ | 127.59 ± 13.68 | $2.23(\pm0.21) \times 10^{49}$ | 49.05 ± 6.49 | $8.86(\pm0.54) \times 10^{50}$ |
| 090516A | 4.109 | $9.96(\pm 1.67) \times 10^{53}$ | 80.75 ± 2.20 | $9.10(\pm 2.26) \times 10^{50}$ | 10.43 ± 2.44 | $7.74(\pm 0.63) \times 10^{51}$ |
| 090812 | 2.452 | $4.40(\pm0.65) \times 10^{53}$ | 77.43 ± 16.6 | $3.13(\pm 1.38) \times 10^{50}$ | 17.98 ± 4.51 | $5.18(\pm 0.61) \times 10^{51}$ |
| 131030A | 1.293 | $3.00(\pm0.20) \times 10^{53}$ | 49.55 ± 7.88 | $6.63(\pm 1.12) \times 10^{50}$ | 33.73 ± 6.55 | $3.15(\pm 0.57) \times 10^{52}$ |
| 140206A | 2.73 | $3.58(\pm0.79) \times 10^{53}$ | 62.11 ± 12.26 | $4.62(\pm0.99) \times 10^{50}$ | 26.54 ± 4.31 | $1.04(\pm 0.59) \times 10^{51}$ |
| 140301A | 1.416 | $9.50(\pm 1.75) \times 10^{51}$ | 276.56 ± 15.50 | $5.14(\pm 1.84) \times 10^{48}$ | 64.52 ± 10.94 | $3.08(\pm0.22) \times 10^{50}$ |
| 140419A | 3.956 | $1.85(\pm 0.77) \times 10^{54}$ | 41.00 ± 4.68 | $6.23(\pm 1.45) \times 10^{50}$ | 14.03 ± 5.74 | $7.22(\pm 0.88) \times 10^{51}$ |
| 141221A | 1.47 | $6.99(\pm 1.98) \times 10^{52}$ | 140.38 ± 5.64 | $2.60(\pm0.64) \times 10^{49}$ | 38.34 ± 9.26 | $7.70(\pm 0.78) \times 10^{50}$ |
| 151027A | 0.81 | $3.94(\pm 1.33) \times 10^{52}$ | 183.79 ± 16.43 | $7.10(\pm 1.75) \times 10^{48}$ | 163.5 ± 30.39 | $4.39(\pm 2.91) \times 10^{51}$ |

Table 1. GRB sample properties of the prompt and flare phases in the cosmological rest frame. This table contains: the redshift z, the isotropic energy E_{iso} , the flare peak time t_p , the flare peak luminosity L_p , the flare duration of which the starting and ending time correspond to half of the peak luminosity Δt , the flare energy E_f within the time interval Δt .

value as E_{iso} . In general, our priority of computing E_{iso} is Fermi, Konus-Wind, then Swift. The energy in the X-ray afterglow is computed in the cosmological rest-frame energy band from 0.3 keV to 10 keV. We smoothly fit the luminosity light-curve using locally weighted regression⁴ which provides a sequence of powerlaw functions. The corresponding energy in a fixed time interval is obtained by summing up all of the integrals of the power-laws within it. In order to take account for the expansion of the Universe, all our computation considers k-correction (Bloom et al. 2001). To compute E_{iso} , the formula for k-correction varies depending on the best fitted model. For the light-curve of X-ray afterglow, k-correction is applied to each light-curve point with a powerlaw spectral index provided by Swift-XRT online repository based on hardness ratio (Evans et al. 2007, 2009). Table. 1 lists the relevant energy value, also it lists the time information of prompt emission, X-ray flare and plateau. The detection of flare's peak is realized by fitting the afterglow data points using also the locally weighted regression, which results in a smooth light-curve, the flare's peak is localized where the tangent of the light-curve has zero slope. The peak time t_{peak} is defined as the time in-

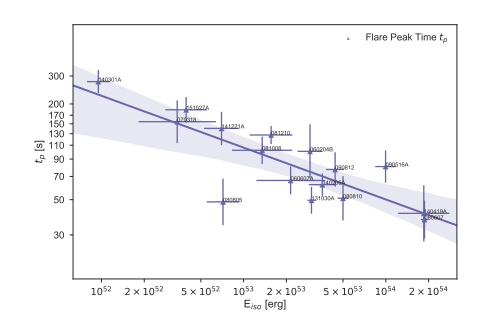


Fig. 2. Relation between E_{iso} and t_p fit by a power-law. The shaded area indicates the 95% confidence level.

terval between the flare's peak and the trigger time, which is satellite dependent, all the sample we refer to *Swift*-BAT. To extract the duration Δt , we work only with the most luminous part of the flare, taking the start time and the end time of the flare at the time when the luminosity is half of the one of the flare peak time.

We then establish correlations between the above quantities characterizing the flare in the beginning of the afterglow with the isotropic energy of the prompt emission. We perform Markov chain Monte Carlo (MCMC) method and iterate 10⁵ times for having the best fit of the power-law and to obtain their correlation

⁴ https://github.com/YWangScience/ AstroNeuron

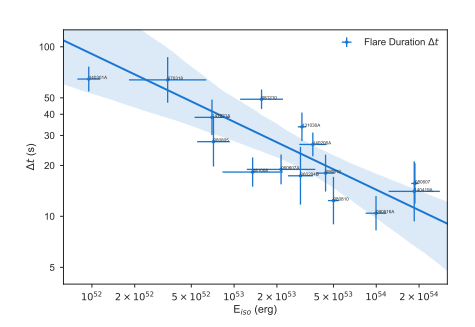


Fig. 3. Relation between E_{iso} and Δt fit by a power-law. The shaded area indicates the 95% confidence level.

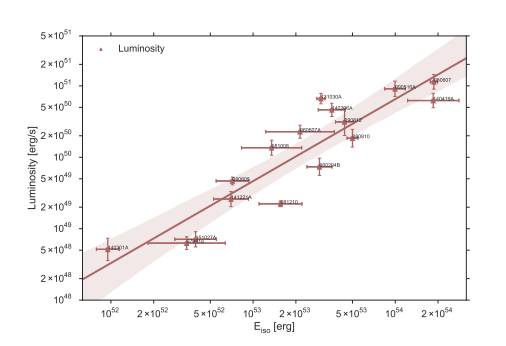


Fig. 4. Relation between E_{iso} and L_p fit by a power-law. The shaded area indicates the 95% confidence level.

| Correlation | Index | Coefficient |
|-----------------------|--------------------|--------------------|
| $E_{iso} - t_p$ | $-0.290(\pm0.010)$ | $-0.764(\pm0.123)$ |
| $E_{iso} - \Delta t$ | $-0.461(\pm0.042)$ | $-0.760(\pm0.138)$ |
| $E_{iso} - L_p$ | $1.186(\pm0.037)$ | $0.883(\pm0.070)$ |
| $E_{iso} - \hat{E_f}$ | $0.631(\pm 0.117)$ | $0.699(\pm 0.145)$ |

Table 2. Power-law correlations among the quantities in Tab. 1. The values and uncertainties (at $1-\sigma$ confidence level) of the power-law index and of the correlation coefficient are obtained from 10^5 MCMC iterations. All relations are highly correlated.

coefficients. The main results are summarized in figures 2–5 and in table 2 ⁵. We find that,

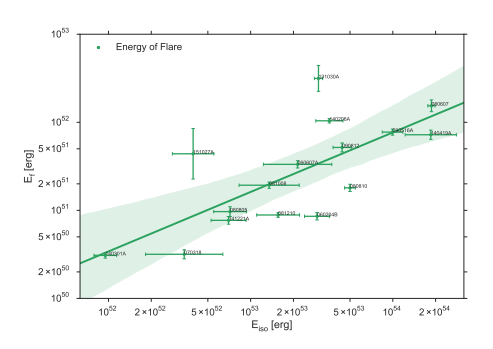


Fig. 5. Relation between E_{iso} and E_f fit by a power-law. The shaded area indicates the 95% confidence level.

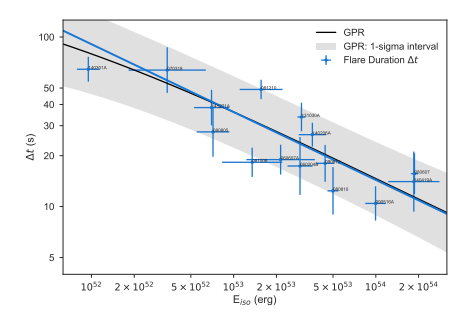


Fig. 6. The GPR fitted curve and its 1-sigma region in black and grey, and the power-law fitting by MCMC in blue (same as figure 3). The GPR curve almost coincides with the power-law line, which indicates the power-law assumption is appropriate.

for our sample that may present flares from a same origin, the peak time t_p , the duration of the flare Δ_t , the peak luminosity L_p and the total energy of flare E_f are highly correlated with isotropic energy E_{iso} , all correlation coefficients are larger than 0.6 (or smaller than -0.6).

In order to verify that if the power-law well describes the correlations, we applied the Gaussian process regression (GPR), which is also an algorithm from machine learning, and it has been pioneeringly introduced to the area of cosmology (Seikel et al. 2012; Yennapureddy & Melia 2017). One example is given in figure 6 for E_{iso} and Δt which are Gaussian dis-

⁵ Codes are uploaded online https://github.com/YWangScience/MCCC

tributed, other features, for example, the velocity of the system, the difference of the environment are considered as noise that also Gaussian distributed but with zero mean. The minimal of the GPR marginal likelihood gives the best fit, meanwhile it gives the noise level $\sim 8\%$. The curve fitted by GPR overlaps with the power-law line, which indicates the power-law assumption is appropriate.

4. Discussion

Many authors have attributed the origin of flares to the long activity of the GRB central engine: one possibility widely discussed is that the central engine produces a series of outgoing shells with a variety of independent Lorentz factors, the collisions between these shells occur over a wide time range, producing the prompt emission and the X-ray flares. (Rees & Mészáros 1994; Fan, Y Z & Wei, D M 2005; Lazzati & Perna 2007; Ghisellini et al. 2007). Beniamini & Kumar (2016) consider the prompt emission and flares are emitted from the photospheres with different Lorentz factors. King et al. (2005); Perna et al. (2006) propose the flares are produced by the continuous or discrete accretion from a surrounding disk. All of these models expect the prompt emission and the afterglow are similar entities but arise independently, no strong correlation should be found. Wang & Dai (2013); Guidorzi et al. (2015) applied the waiting time statistics, a common stochastic model was found to describe the prompt emission and the afterglow. This stochasticity in principle also shall lead to the independency of observational quantities between the prompt emission and the X-ray flare. But for our sample, although the prompt emission and the afterglow are two distinct phases, they are strictly correlated, there exists many correlations between the energy (E_{iso}) of the prompt emission and the energy (E_{flare}) , time (t_{peak}) , duration (Δt) of the flare. This discrepancy probably not come from the selection effect of our sample, since our criteria do not eliminate the randomness from the assumed central engine models. First all the criteria are apparently independent; second in the aforementioned papers, the characteristic parame-

ters of criteria have not been independently found any correlations with the characteristic variables of the models (Lorentz factor, accretion mass and etc); third, we don't specifically select some GRBs, our criteria make general divisions. Since the discrepancy is not from the selected data, we may state the long and random activity of central engine are not the solution for our sample. Furthermore, we are bold to propose that the observed stochasticity for a general selection of flares is not appropriately interpreted by different Lorentz factors or other characteristics within a specific mechanism, but flares could have many different origins, the statistical analysis adopting a mixture of flares with different origins fuzz up the intrinsic patterns and brings the stochastic appearance. The sample we selected may present one of the mechanisms, and the correlations indicate this mechanism of producing flares is highly related to the prompt emission, that the prompt emission and the X-ray flare may occur in a same sequence.

These correlations indicates the properties of central engine, moreover themselves have important applications: the prompt emission and afterglow are observed independently, the correlations we found bridge them, therefore, for GRBs without complete observation, our correlations can be used to infer the missing information; for GRBs with complete data, we can apply our correlations for the cosmology.

The launch of THESUS satellite⁶ will open our vision to the macroscopic early universe, as well as the microscopic details of the infra-red, X-ray and gamma-ray spectra. It will increase numerously the GRB sample for the statistics, also it will investigate deeply the commonalities and the differences between GRB components. In this paper, in order to understand the physics of GRBs, we adopted a novel perspective to study statistically the correlations between the prompt emission and the X-ray flare, the THESUS satellite perfectly suites our purpose, it will definitely promote our understanding to a higher stage.

Official website: http://www.isdc.unige.ch/theseus/

References

- Ackermann, M., Ajello, M., Asano, K., et al. 2013, ApJS, 209, 11
- Beniamini, P., & Kumar, P. 2016, MNRAS, 457, L108
- Bloom, J. S., Frail, D. A., & Sari, R. 2001, AJ, 121, 2879
- Chincarini, G., Moretti, A., Romano, P., et al. 2007, ApJ, 671, 1903
- Curran, P. A., Starling, R. L. C., O'Brien, P. T., et al. 2008, A&A, 487, 533–538
- Dezalay, J.-P., Barat, C., Talon, R., et al. 1992, in American Institute of Physics Conference Series, Vol. 265, American Institute of Physics Conference Series, ed. W. S. Paciesas & G. J. Fishman, 304–309
- Evans, P. A., Beardmore, A. P., Page, K. L., et al. 2007, A&A, 469, 379
- —. 2009, MNRAS, 397, 1177
- Fan, Y Z, & Wei, D M. 2005, MNRAS, 364, L42
- Ghisellini, G., Ghirlanda, G., Nava, L., & Firmani, C. 2007, ApJ, 658, L75
- Guidorzi, C., Dichiara, S., Frontera, F., et al. 2015, ApJ, 801, 57
- King, A., O'Brien, P. T., Goad, M. R., et al. 2005, ApJ, 630, L113
- Kouveliotou, C., Meegan, C. A., Fishman, G. J., et al. 1993, ApJL, 413, L101
- Lazzati, D., & Perna, R. 2007, MNRAS, 375, L46
- Lien, A. Y., Barthelmy, S. D., Chester, M. M., et al. 2014, GRB Coordinates Network, 15784
- Malesani, D., Xu, D., Fynbo, J. P. U., et al. 2014, GRB Coordinates Network, 15800
- Perna, R., Armitage, P. J., & Zhang, B. 2006, ApJ, 636, L29
- Rees, M. J., & Mészáros, P. 1994, ApJ, 430, L93–96
- Ruffini, R., Aimuratov, Y., Bianco, C. L., et al. 2015, IJMPA, 30, 1545023
- Ruffini, R., Rueda, J. A., Muccino, M., et al. 2016, ApJ, 832, 2
- Ruffini, R., Wang, Y., Aimuratov, Y., et al. 2018, ApJ, 852, 53
- Sakamoto, T., Barthelmy, S. D., Baumgartner,W. H., et al. 2014, GRB CoordinatesNetwork, 15805

- Seikel, M., Clarkson, C., & Smith, M. 2012, JCAP, 6, 036
- Swenson, C. A., Roming, P. W. A., de Pasquale, M., & Oates, S. R. 2013, ApJ, 774, 2
- Wang, F. Y., & Dai, Z. G. 2013, Nature Physics, 9, 465
- Yennapureddy, M. K., & Melia, F. 2017, JCAP, 11, 029
- Zhang, B., Fan, Y Z., Dyks, J., et al. 2006, ApJ, 642, 354